⌘ *Author's Choice*

Peptide-Major Histocompatibility Complex Dimensions Control Proximal Kinase-Phosphatase Balance during T Cell Activation[S]

Kaushik Choudhuri[‡1,2], **Mathew Parker**[§3,4], **Anita Milicic**[¶], **David K. Cole**[‖], **Michael K. Shaw**[‡], **Andrew K. Sewell**[‖],
Guillaume Stewart-Jones[**], **Tao Dong**[**], **Keith G. Gould**[§3,5,6], and **P. Anton van der Merwe**[‡1,5,7]

From the [‡]Sir William Dunn School of Pathology, the [¶]Jenner Institute, and the [**]Medical Research Council Human Immunology Unit, Weatherall Institute of Molecular Medicine, University of Oxford, Oxford OX1 3RE, United Kingdom, the [§]Department of Immunology, Wright-Fleming Institute, Imperial College London, London W2 1PG, United Kingdom, and the [‖]Department of Medical Biochemistry and Immunology, School of Medicine, Cardiff University, Cardiff CF14 4XN, United Kingdom

T cell antigen recognition requires binding of the T cell receptor (TCR) to a complex between peptide antigen and major histocompatibility complex molecules (pMHC), and this recognition occurs at the interface between the T cell and the antigen-presenting cell. The TCR and pMHC molecules are small compared with other abundant cell surface molecules, and it has been suggested that small size is functionally important. We show here that elongation of both mouse and human MHC class I molecules abrogates T cell antigen recognition as measured by cytokine production and target cell killing. This elongation disrupted tyrosine phosphorylation and Zap70 recruitment at the contact region without affecting TCR or coreceptor binding. Contact areas with elongated forms of pMHC showed an increase in intermembrane distance and less efficient segregation of CD3 from the large tyrosine phosphatase CD45. These findings demonstrate that T cell antigen recognition is strongly dependent on pMHC size and are consistent with models of TCR triggering requiring segregation or mechanical pulling of the TCR.

T cell antigen recognition requires the engagement of the TCR[8] with peptide antigen presented on cell surface MHC mol-

ecules (pMHC) (1). "Accessory" T cell surface receptors modulate T cell antigen recognition by binding to cell surface ligands on antigen-presenting cells (APCs) (2). The dimensions of the TCR·pMHC complex dictate that TCR binding to pMHC takes places within close contact areas in which the membranes are ~15 nm apart (3–5). Many accessory receptor·ligand complexes span similar dimensions to the TCR·pMHC complex and can therefore colocalize with the TCR in such close contact areas (3–5). Conversely, many cell surface molecules, including two of the most abundant, CD43 and CD45, have much larger ectodomains and would therefore be expected to be excluded or depleted from these close contact areas (3, 6).

Signal transduction by the TCR is mediated by the associated CD3 subunits (7). The earliest event that is known to be required for signaling is tyrosine phosphorylation of immunoreceptor tyrosine-based activation motifs in the cytoplasmic portion of these TCR-associated CD3 subunits. This phosphorylation, which is mediated by Src-related kinases such as Lck, is followed by recruitment and activation of the tyrosine kinase Zap70 (which binds doubly phosphorylated immunoreceptor tyrosine-based activation motifs via tandem SH2 domains). Zap70 then phosphorylates downstream proteins, including adaptor proteins such as LAT and SLP-76, leading to the recruitment and activation of a cascade of adaptor and effector proteins (2). Although the downstream events in TCR signal transduction are fairly well characterized, the mechanism by which TCR binding to pMHC leads to increased phosphorylation of CD3 immunoreceptor tyrosine-based activation motifs, a process termed TCR triggering, remains relatively poorly understood and controversial (8–13).

A number of models have been proposed for TCR triggering. These can be classified into three groups depending on whether the signal transduction mechanism involves aggregation, conformational change, or segregation of the TCR·CD3 complex upon pMHC binding (reviewed in Ref. 14). Models based on aggregation have difficulty accounting for TCR triggering by very low densities of agonist pMHC, so recent versions postulate a role for self-pMHC, which is present at higher densities (8). Models postulating conformational change within TCR$\alpha\beta$

have not generally been supported by structural studies (15) and so have been adapted by proposing conformational changes of the entire TCR$\alpha\beta$ complex with respect to other components or the plasma membrane (14, 16). A version of these models proposed that conformational change may be the result of pMHC binding subjecting the TCR to a mechanical "pulling" force toward the APC membrane (14, 16, 17). However, very recently evidence has been presented that binding to agonist pMHC may indeed trigger a conformational change within the constant domain of the TCR$\alpha\beta$ (18), so that models based on conformational change need to be reassessed. In addition, conformational changes in the cytoplasmic domains of the TCR-associated CD3 polypeptides may help to regulate TCR activation (19). Finally, TCR triggering models based on segregation postulate that TCR binding to pMHC functions to retain the TCR·CD3 components within a region of the plasma membrane within which tyrosine kinases such as Lck are enriched and receptor tyrosine phosphatases are depleted. The kinetic segregation model postulates that this segregation is the result of the large size of the ectodomain of tyrosine phosphatases CD45 and CD148 with respect to the TCR·pMHC complex, which leads to physical exclusion from close contact areas (6, 9, 20).

To explore the mechanism of TCR triggering, we have examined whether the small size of the TCR·pMHC complex is functionally significant. We showed previously that elongation of one mouse pMHC class I complex abrogated recognition by cognate T cells (21). The present study extends this previous work in several important ways. First, we extend this analysis to other pMHC complexes and cognate T cells, including human CD8 T cells. Second, we test directly whether the inhibitory effect could be the result of decreased TCR or coreceptor binding to elongated pMHC class I. Third, we look at the effect of pMHC elongation on early signaling events and segregation of CD45 from TCR·CD3 within the contact area. Our results conclusively demonstrate the importance of pMHC size in T cell antigen recognition and are consistent with the kinetic segregation model of TCR triggering.

EXPERIMENTAL PROCEDURES

Constructs and Protein Expression—The H-2D^b and HLA-A2 single-chain trimer (SCT) constructs are analogous to the SCT we have described previously for H-2K^b (21). The H-2D^b SCT presents the peptide epitope ASNENMDAM (NT60), residues 366–374 of influenza virus A/NT/60/68 nucleoprotein (22), and the HLA-A2 SCT presents the peptide epitope SLYNTVATL, residues 77–85 of human immunodeficiency virus, type 1 Gag p17. The H-2D^b SCT construct uses murine β_2-microglobulin, and the HLA-A2 SCT uses human β2-microglobulin. The SCT constructs were expressed in transfected cells from the SV40 early promoter, using expression vectors pKG4 or pKG5. To obtain cells with low levels of surface SCT expression, a tetracycline-inducible expression system consisting of the vector pcDNA5/TO and T-Rex-CHO (Chinese hamster ovary) cells (Invitrogen) was used in the absence of tetracycline. The strategy to generate elongated SCT chimeras was exactly as described (21), using an introduced unique BamHI restriction site in the class I heavy chains. This enabled the use of the identical CD2, CD22, and CD4 inserts used previously, adding two, three, and four extra Ig-like domains, respectively. For the HLA-A2 SCT, only a CD4-extended version was made.

Soluble versions of the HLA-A2 SCT proteins were made by removing the transmembrane and cytoplasmic regions. For the unextended soluble SCT, the HLA-A2 heavy chain terminates at residue Trp^{274}. For the CD4-extended soluble SCT, Trp^{274} is followed by the sequence EDPPS before continuing with the CD4 insert. Both constructs then contain additional residues at the C-terminal end, comprising a Myc epitope tag, a biotinylation sequence, and a His$_6$ tag to facilitate purification. The amino acid sequence of this region is TGEQKLISEEDLGLN-DIFEAQKIEWHHHHHH. For expression, the constructs were cloned into the bicistronic retroviral expression vector pQCXIX (Clontech). The second multiple cloning site of the vector was used to express green fluorescent protein. Pantropic recombinant retrovirus was produced by transient transfection of the GP2–293 packaging cell line with the recombinant pQCXIX plasmids and pVSV-G vector (Clontech). Tissue culture supernatant containing retrovirus was used to infect 293T cells; multiple rounds of infection were carried out, and the level of infection was monitored by the level of green fluorescent protein expression. Once high levels of infection had been achieved (five or six rounds of infection), clones were made by limiting dilution. The clones that demonstrated very high levels of green fluorescent protein expression were tested by Western blotting for SCT protein expression in culture supernatant. The best expressing clones were expanded, and SCT protein was purified from culture supernatant using Ni^{2+}-nitrilotriacetic acid-agarose (Qiagen). Protein was eluted with a gradient of imidazole, desalted into 10 mM Tris buffer, pH 7.5, and biotinylated using recombinant BirA enzyme according to the manufacturer's instructions (Avidity LLC). Biotinylated SCTs were purified by gel filtration (fast protein liquid chromatography) using Superdex 75 or 200 columns and stored in PBS. Biotinylation efficiency was checked by depletion assay in which 10 μl of streptavidin-coupled magnetic beads (Dynal) were incubated with 10 ml of SCTs (5 μg) for 20 min at room temperature, after which supernatant was separated by 10% SDS-PAGE and protein was detected by Coomassie staining.

Human CD8$\alpha\alpha$ was expressed and purified as described elsewhere (23). The concentration of CD8$\alpha\alpha$ was determined using an extinction coefficient of 32,480 M^{-1} cm^{-1}. Human G10 TCR was expressed and refolded *in vitro* as described (24), and concentration was determined using an extinction coefficient of 63,995 M^{-1} cm^{-1}.

T Cells—Splenocytes were harvested from F5 RAG$^{-/-}$ mice, primed with 10 μM NT60 peptide for 48 h, and purified by negative selection and Ficoll (Sigma) separation (>95% CD8+) before culturing for a further 6 days in complete medium containing 20 units/ml recombinant murine IL-2 (Sigma). The cells were rested in complete medium without IL-2 for 2 h prior to use in stimulation assays in which 10^4 T cells/well were incubated with varying numbers of SCT-expressing CHO cells (denoted as APC/F5 ratio). Culture supernatants were assayed for IL-2 by ELISA after incubation at 37 °C in 5% CO$_2$ for 24 h. Alternatively, an F5 TCR-expressing CD8$^+$ murine T cell clone

(F5 CTL), propagated by several rounds of antigen-induced expansion, was incubated for 6 days with syngeneic B6 splenocytes loaded with 10 μM NT60 peptide in medium containing 100 units/ml recombinant murine IL-2. Viable lymphocytes were isolated by Ficoll gradient centrifugation. The cells were rested for 4 days in medium containing 20 units/ml IL-2 and used at day 10 post-priming. For human G10 CD8+ T cells, the well established G10 clone (24) was expanded using irradiated heterologous peripheral blood mononuclear cells from three donors in the presence of IL-2. Viable cells were isolated on day 14 post-priming and used on the same day. The SLY10 T cell clone was cultured in human IL-15-containing medium for 24 h and used as above in stimulation assays. The B3Z murine T cell hybridoma (expressing the OT1 TCR) was used as a control for SCT accumulation by F5 RAG$^{-/-}$ cells.

Confocal Immunofluorescence Microscopy—For imaging of G10 T cells, coverslips were cleaned by overnight incubation in 1 N HCl at 60 °C, followed by graded hydration by sonication in an ethanol series (95, 70, 50, 25, and 0%). Following brief coating with 0.01% poly-L-lysine, the coverslips were washed and coated with 0.05 mg/ml streptavidin in PBS (Sigma) for 2 h at 37 °C. Biotinylated SCTs (10 μg/ml in PBS) were immobilized onto coated coverslips by incubation for 1 h at room temperature. As a control, the coverslips were coated with 10 μg/ml biotinylated mouse anti-human HLA class I antibody (W6/32; Abcam). Following washing, G10 T cells in complete RPMI medium were incubated on coverslips for 1 min at 37 °C in 5% CO_2. The medium was aspirated, and the cells were fixed in 2% paraformaldehyde for 10 min at 37 °C and permeabilized for 5 min in 0.05% Triton X-100. The samples were stained for CD3ϵ, Zap70, and CD45 by serial incubation of each antibody followed where appropriate by a species-specific and fluorophore-conjugated secondary antibody in the order mouse anti-CD3ϵ (UCHT1; AbD Serotec), anti-mouse Alexa 488 (Molecular Probes), rabbit anti-Zap70 (99F2; Cell Signaling Technology), anti-rabbit IgG Alexa 546 (Molecular Probes), and anti-human pan CD45 antibody directly conjugated with Alexa 647 (F10-89-4; AbD Serotec). The samples were washed extensively between all steps and sealed in anti-fade containing mounting agent (Molecular Probes). The images were acquired on a Zeiss LSM Pascal laser scanning confocal microscope equipped with 488/543/633 laser lines using the appropriate excitation and bandpass emission filters. The coverslip surface was identified by the second maxima of reflected light, and 1024 $\times$ 1024 pixel images were acquired using a Planapochromat $\times$63, NA 1.4 oil objective. A pinhole diameter corresponding to an optical slice thickness of 0.5 μm was chosen for imaging cell/glass interface-associated fluorescence. Multiple experiments were performed using identical labeling and imaging parameters.

Cell conjugates for phoshotyrosine labeling were prepared by brief centrifugation at 4 °C of equal numbers of primed F5 RAG$^{-/-}$ T cells and SCT-expressing CHO cells labeled with a far-red emitting dye (DDAO; Molecular Probes). Following incubation at 37 °C for 2 min, the cells were fixed and permeabilized on glass coverslips. The samples were labeled with anti-phosphotyrosine antibody conjugated with Alexa 488 (G10; Santa Cruz Biotechnology) and prepared as above for imaging by confocal immunofluorescence microscopy. A similar method was used for imaging SCT accumulation. Conjugates of F5 RAG$^{-/-}$ or B3Z T cells, labeled with DDAO, and SCT-expressing CHO cells were labeled with a mouse anti-H2-D^b monoclonal antibody (27-11-13S) followed by anti-mouse secondary conjugated with fluorescein isothiocyanate (BD Pharmingen).

Image Processing and Data Analysis—The Metamorph and ImageJ software packages were used for all image processing, and ImageJ was used for calculation of the Manders coefficient. All of the images were background subtracted prior to analysis. Interface enrichment was calculated as previously described using Metamorph (21).

Transmission Electron Microscopy—Conjugates were fixed in a mixture of 2.5% glutaraldehyde and 2% formaldehyde in 100 mM cacodylate buffer, pH 7.4, with 2 mM Ca^{2+}, post-fixed in buffered 1% osmium tetroxide and en bloc stained with 0.5% aqueous uranyl acetate. Ultrathin ($\sim$60 nm thick) were cut and double stained with uranyl acetate and led citrate. All of the sections were examined in a Zeiss (LEO) Omega 912 electron microscope (Zeiss/LEO Electron Microscope Ltd., Oberkochen, Germany) equipped with a Proscan CCD camera (2048 by 2048 pixels). Digital images were captured with the integrated Soft Imaging Software image analysis package (Soft Imaging Software, GmbH, Münster, Germany), and absolute measurements were recorded directly from the images. Interfaces were imaged at $\times$35,500 magnification, and intermembrane distances were measured (at a 200% digital magnification) where apposed membranes were aligned (parallel) and where both membranes exhibited a trilaminar appearance, indicating that they were orthogonal to the image plane.

T Cell Activation Assay—Primed T cells (F5 RAG$^{-/-}$ or G10) in complete RPMI medium were placed in 96-well round-bottomed microtitre plates at 10^4 cells/well with varying numbers of CHO cells expressing native and elongated SCTs, represented in figures as T cell/APC ratio. The cells were incubated for 24 h at 37 °C in 5% CO_2, and culture supernatants were collected for cytokine measurements. For PP2 inhibitor experiments, T cells were incubated with PP2 (Calbiochem) for 30 min, washed, and plated at 10^4 cells/well with CHO cells expressing native SCT at 5×10^4 cells/well and processed as described above. Equivalent amounts of PP2 corresponding to concentrations for T cells were added to CHO cells just before addition to microtitre wells to maintain overall PP2 concentrations.

ELISA—For IL-2 measurements, culture supernatants and mouse recombinant IL-2 standards (Sigma) were incubated in microtitre plates coated with a capture anti-mouse IL-2 antibody (BD Pharmingen) for 2 h at 37 °C, washed, and incubated for another 1 h with a biotinylated detection anti-mouse IL-2 antibody (BD Pharmingen). Following extensive washing, the plates were incubated with extravidin-horseradish peroxidase for 30 min and developed using 3,3′,5,5′-tetramethylbenzidine substrate (Sigma). Absorbance was measured at 450 nm in a spectrophotometric plate reader, and IL-2 concentration was interpolated from the absorbance of IL-2 standards. Commercially available ELISA kits employing a similar sandwich ELISA method were used for detection of human IFNγ (BD Pharmin-
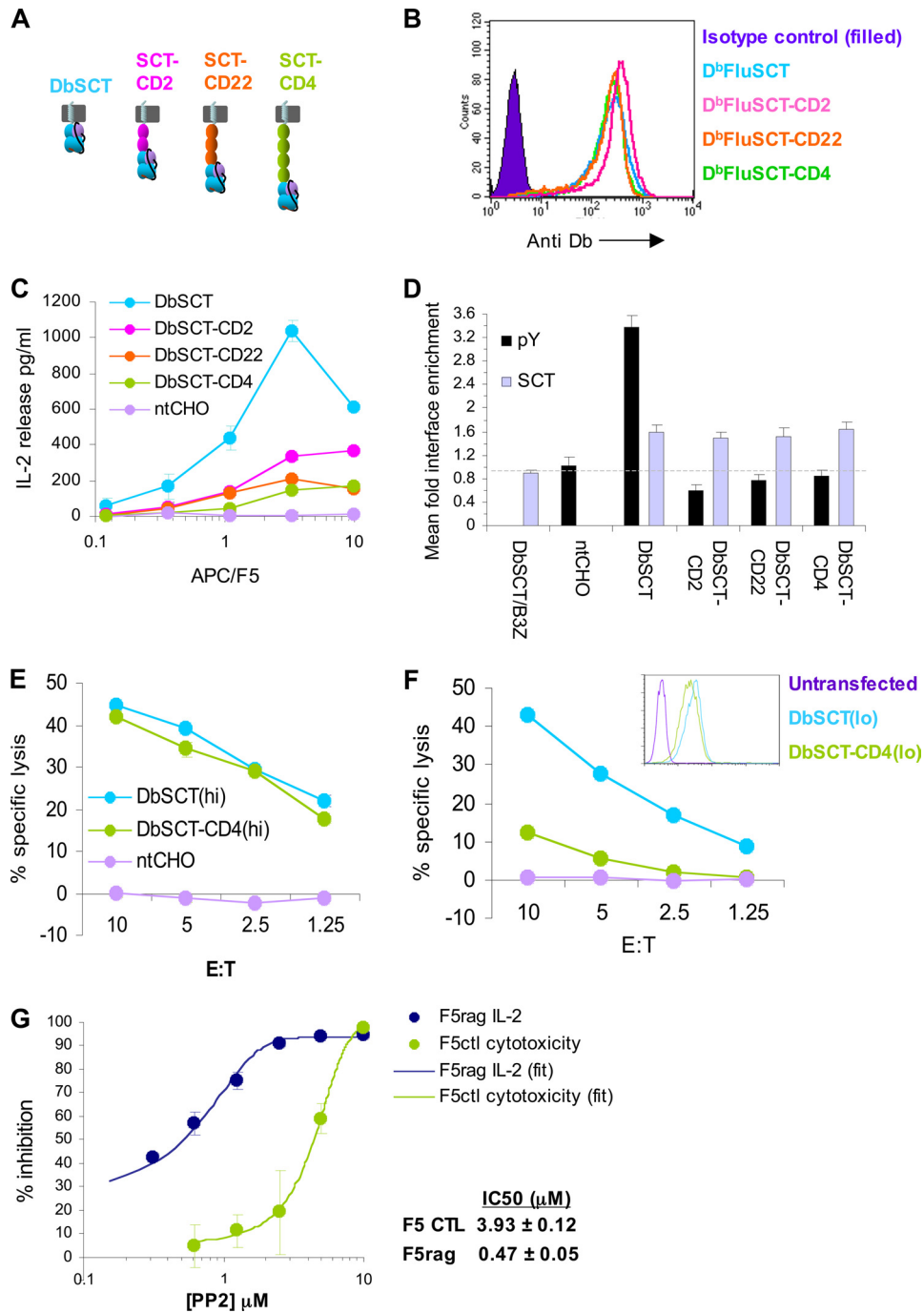
FIGURE 1. **T cell receptor triggering and effector responses are abrogated by pMHC elongation in a murine system.** *A*, schematic representation of native and elongated versions of D^{b}SCT containing the indicated membrane-proximal IgSF spacers, tethered to the plasma membrane by the native H-2D^b stalk and transmembrane segments. *B*, surface expression levels of SCT constructs in TAP2-deficient CHO cells. *C*, primed transgenic T cells expressing the F5 TCR (10^4 T cells/well) were incubated with varying numbers of SCT-expressing CHO cells (denoted as APC/F5 ratio). Culture supernatants were assayed for IL-2 by ELISA after 24 h of incubation. A representative plot of three independent experiments is shown. The *error bars* represent ± S.D. *D*, F5/APC conjugates were incubated for 2 min at 37 °C before fixing and stained for phosphotyrosine and H-2D^b (SCTs). The conjugates were imaged by confocal immunofluorescence microscopy (Fig. S1A). Untransfected CHO cells were used to determine basal phosphorylation levels. Phosphotyrosine accumulation at the T cell interface was quantified as the ratio of interface/noninterface fluorescence (*black bars*). At least 25 conjugates were randomly chosen for analysis. Accumulation of SCTs was measured using a similar approach (supplemental Fig. S1B). As a control, conjugates of B3Z hybridomas expressing the noncognate OT1 TCR and CHO cells expressing D^{b}SCT were used. Accumulation of SCT at the interface was quantified for 19–25 randomly chosen conjugates for each SCT (*purple bars*). The *error bars* represent S.E. The *dashed line* represents enrichment ratio of 1 (no enrichment) *E*, fully differentiated F5 CTL were assessed for sensitivity to elongated pMHC expressed at high levels (as in *B*) on CHO cells. Cytotoxic responses of F5 CTL to SCTs was tested in a 6-h ^{51}Cr release assay using CHO cells expressing native and maximally elongated (SCT-CD4) SCTs as targets. The data are representative of two independent experiments. The *error bars* represent ± S.D. *F*, cytotoxic responses by F5 CTL to low levels (~50-fold lower than cells shown in *B*) of SCT expression (*inset*). The data are representative of two independent experiments. *G*, cytolytic activity of F5 CTL and IL-2 release by F5 RAG$^{-/-}$ T cells in response to high levels of SCT expression (as in *B*) in the presence of 0–10 μM PP2 was measured as in *C* and *E*. The data are expressed as the percentages of reduction in response relative to responses in the absence of PP2. The concentration of PP2 that gave 50% inhibition (IC$_{50}$) was derived from error-weighted sigmoidal fitting of the data. The *error bars* represent ± S.D.

Antigen Recognition Outcome Depends on pMHC Size

TABLE 1

pMHC elongation increases the average intermembrane distance at the T cell/APC interface

Mean intermembrane distances measured as described in supplemental Fig. S2 were compared by analysis of variance with correction for multiple comparisons.

	Average intermembrane distance (±S.D.)	No. of measurements	No. of conjugates	Comparison	p
	nm				
D^bSCT	13.1 (3.1)	98	20	D^bSCT *vs.* D^bSCT-CD2	<0.05
D^bSCT-CD2	14.4 (3.5)	109	20		
D^bSCT-CD4	18.9 (5.3)	130	25	D^bSCT-CD4 *vs.* D^bSCT/D^bSCT-CD2	<0.01

gen) and MIP1b (R & D Systems), according to the manufacturers' instructions.

Cytotoxicity Assay—A standard 5- or 6-h ^{51}Cr release assay was used to measure cytotoxicity. CHO target cells were detached using PBS containing 0.5 mM EDTA and labeled in RPMI medium with ^{51}Cr Na_2CrO_4 (MP Biomedicals) for 1 h at 37 °C. After two washes, target cells were plated out in round-bottomed 96-well plates at 10,000 cells/well with F5 CTL effectors at the indicated effector to target ratios, in a total volume of 150 μl. The medium for the assay was complete RPMI + 10% fetal calf serum + 10 mM HEPES buffer, pH 7.4. After 5 or 6 h at 37 °C supernatant from each well was harvested, and ^{51}Cr release was determined. The percentage specific lysis was calculated as follows: $100 \times$ (release by CTL − medium release)/ (3.3% Triton release − medium release). Each point was measured at least in duplicate against quadruplicate controls. Spontaneous release was less than 20% of Triton release in all experiments. For PP2 inhibition of CTL, target cells expressing a high level of H-2D^b SCT were used with F5 CTL at an E:T target ratio of 10:1, and PP2 was included during the 5-h release period at concentrations from 0 to 10 μM. The CTL were preincubated with PP2 for 30 min before the target cells were added. PP3 was used as a control in the same experiment and gave no inhibition of lysis (data not shown).

Surface Plasmon Resonance—To ensure that proteins were monomeric, frozen aliquots of CD8$\alpha\alpha$ and SCTs were purified by gel filtration on the day of experiments. Binding measurements were performed on a BIAcore 2000 instrument. Biotinylated SCTs were immobilized at ~500 response units on streptavidin-coupled CM5 chips, and doubling dilutions of 154 μM CD8$\alpha\alpha$ were injected over flow cells at 50 μl/min. G10 TCR binding to immobilized SCTs was measured similarly over a 0.1–7 μM concentration range. Binding curves were extracted and analyzed as described previously (23).

Statistical Analysis—Two-tailed T tests assuming unequal variance, one-way analysis of variance with Bonferroni's correction, and nonlinear curve fittings were performed using PRISM software.

RESULTS

Elongation of H-2D^b Abrogates Antigen Recognition by F5 T Cells—We first examined the effect of elongation of the mouse MHC class I molecule H-2D^b on pMHC recognition by T cells expressing the F5 TCR, derived originally from influenza virus-infected mice (25). To avoid confounding the effects of elongation on peptide loading and/or assembly, the peptide epitope comprising residues 366–374 of influenza virus A/NT/60/68 nucleoprotein, β2-microglobulin, and H-2D^b heavy chain were covalently joined by glycine/serine linkers and expressed as a

single-chain trimer (D^{b}SCT) (21, 22). Elongated forms of D^{b}SCT were generated by the insertion of two, three, or four Ig domains from the ectodomains of CD2, CD22, and CD4 into the stalk region (Fig. 1A), and artificial APCs generated expressing comparable surface levels of these proteins on transporter associated with antigen processing (TAP)-deficient CHO cells (Fig. 1B). Incubation of T cells from F5 TCR transgenic mice with APCs expressing D^{b}SCT resulted in IL-2 release, indicating specific recognition of the D^{b}SCT by the F5 TCR (Fig. 1C). APCs expressing elongated forms of D^{b}SCT stimulated considerably less IL-2 production, with the extent of IL-2 release correlated inversely with D^{b}SCT size.

To investigate early signaling events, we visualized phosphotyrosine accumulation at the contact interface in T cell/APC conjugates (supplemental Fig. S1A). An increase in interface phosphotyrosine was observed with D^{b}SCT-expressing *versus* control CHO APCs, but no such increase was seen in conjugates with CHO cells expressing elongated D^{b}SCT (Fig. 1D). We also measured D^{b}SCT enrichment at the contact interface as a measure of TCR engagement (supplemental Fig. S1B). Elongated forms of D^{b}SCT were enriched to the same extent as normal length D^{b}SCT (Fig. 1D), indicating that elongation did not disrupt TCR binding. Finally, we used transmission electron microscopy to show that elongation of D^{b}SCT increased the intermembrane distance at the contact interface between F5 T cells and D^{b}SCT-expressing CHO cells (Table 1). It was notable, however, that the increase was significantly less than might be expected by the size of the inserts (~7 nm for CD2 and ~12 nm for CD4). This result, taken together with the finding that the intermembrane distance was more variable as the insert length increased (Table 1 and supplemental Fig. S2), suggests that the constructs were flexible and not fully extended at the interface.

While performing other functional assays involving T cell antigen recognition, we found that fully differentiated cytotoxic F5 T cells killed CHO cells expressing elongated D^{b}SCT as effectively as cells expressing nonelongated D^{b}SCT (Fig. 1E). One possible explanation is that induction of killing by CD8 T cells has a lower activation threshold than other effector functions such as IL-2 secretion (26–28); indeed even a single pMHC on a target cell can be sufficient to induce killing (29). This was supported by the observation that lysis of CHO cells expressing much lower levels of D^{b}SCT was inhibited by elongation of D^{b}SCT (Fig. 1F). Consistent with this, we found that ~10-fold higher concentrations of the tyrosine kinase inhibitor PP2 were required to inhibit killing compared with IL-2 production (Fig. 1G).
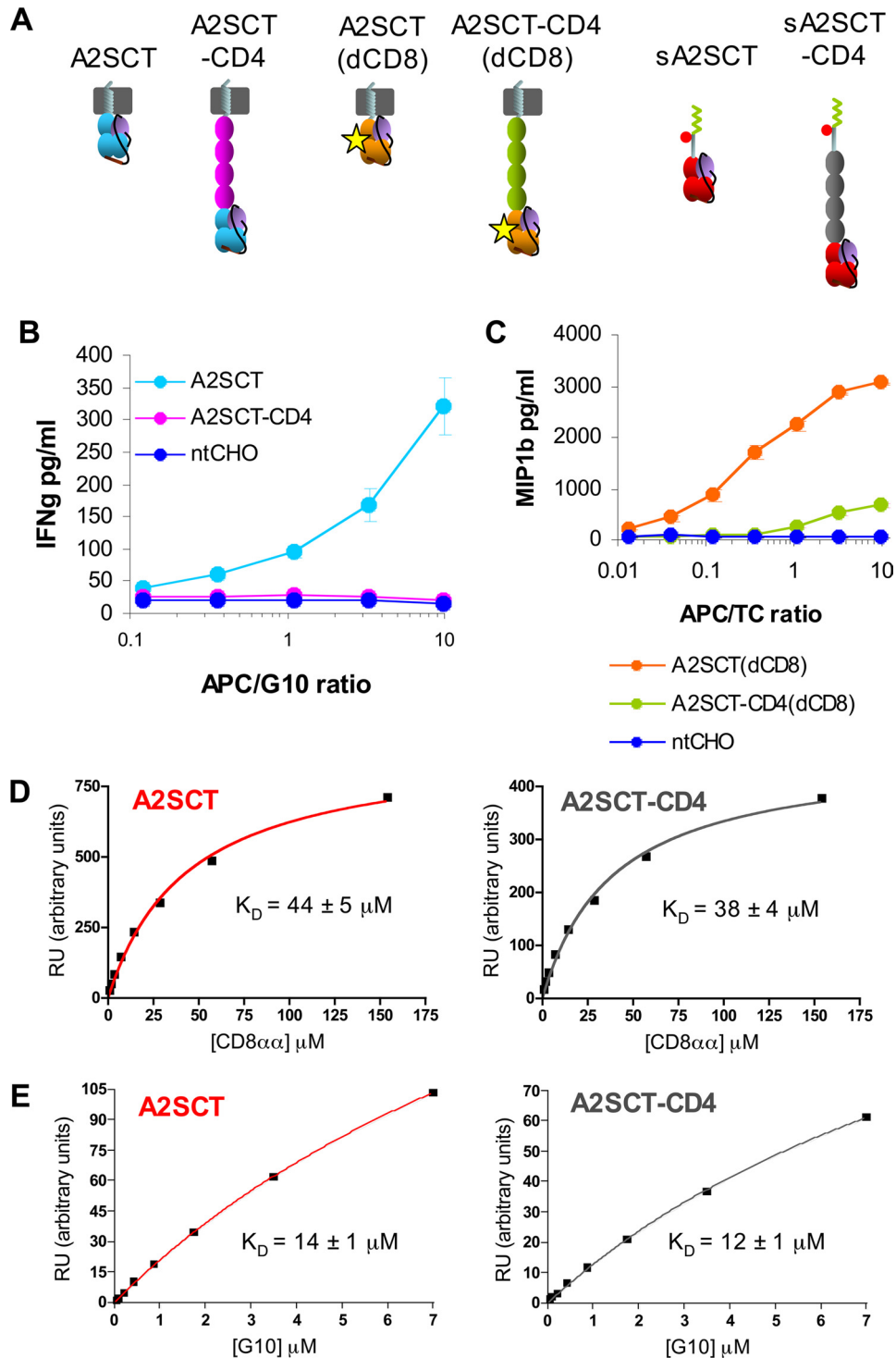
FIGURE 2. **Elongation of a human pMHC (gagSLY/HLA-A2) abrogates activation of G10 T cells expressing cognate TCR.** *A*, schematic representation of single-chain constructs of native and elongated single-chain versions of HLA-A2/gag and corresponding coreceptor binding mutants (*yellow stars*). Constructs were stably expressed in TAP2-deficient CHO cells and sorted for comparable expression for use as surrogate antigen-presenting cells (supplemental Fig. S3*A*). Also shown are soluble forms of native and elongated constructs comprising the extracellular portion followed by a C-terminal biotin acceptor site (*red dot*) and His$_6$ tag (*green line*). *B*, activation of primed G10 T cells was assessed by incubating 10^4 G10 cells/well with varying numbers of SCT-expressing APC (denoted as APC/G10 ratio) and IFNγ release measured by ELISA of culture supernatants after 8 h incubation. A representative plot of three independent experiments is shown. *C*, the human T cell clone SLY10 was used to assess responses to SCTs with mutated coreceptor-binding sites. Varying numbers of SCT-expressing CHO cells were incubated with 10^4 SLY10 cells/well, and MIP1b release was measured by ELISA of culture supernatants after 24 h of incubation. *D*, coreceptor binding to native and elongated SCTs was assessed by surface plasmon resonance (BIAcore). Monomeric biotinylated SCTs were immobilized by coupling to streptavidin conjugated CM5 flow cells (~500 reference units). Binding curves were obtained by injecting CD8$\alpha\alpha$ at a range of concentrations (0.9–154 μM) over flow cell surfaces immobilized with native or elongated SCTs. Immobilized biotinylated polyclonal anti-hamster IgG antibody was used as a control surface. The experiments were performed at 25 °C at a flow rate of 5 μl/min. Plateau response units were plotted against CD8$\alpha\alpha$ concentration, and K_D values were obtained by nonlinear curve fitting. The data are representative of two independent experiments. *E*, binding of native and elongated SCTs to G10 TCR was compared by surface plasmon resonance as described for *D*. The binding curves were obtained by injecting G10 TCR (0.1–7 μM) over immobilized SCTs, HLA-A2/NY-ESO, in addition to an irrelevant antibody-bound control surface.
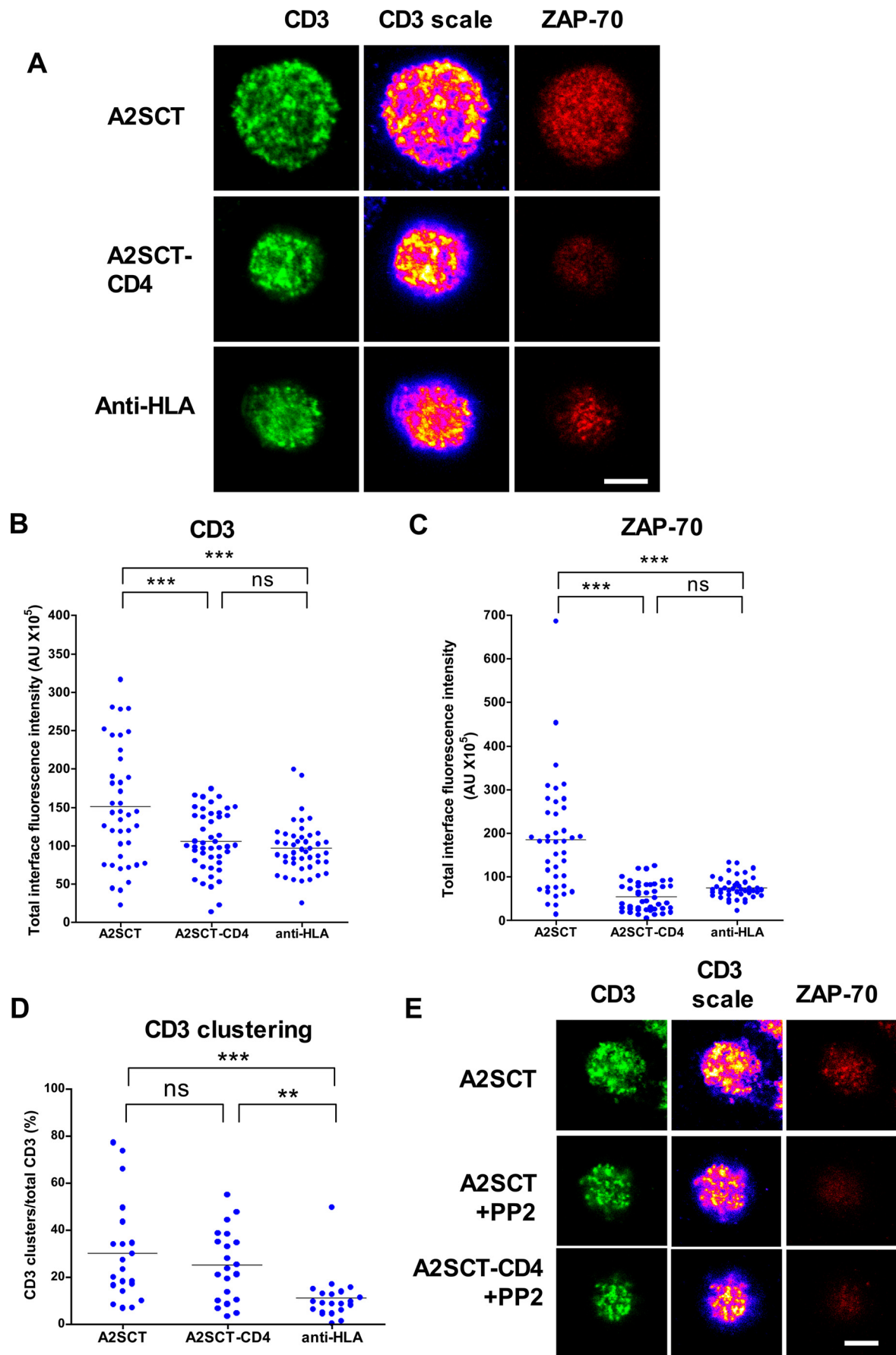
Elongation of HLA-A2 Abrogates Antigen Recognition without Affecting Coreceptor Binding—These results and our previous report confirmed that antigen recognition by mouse CD8 T cells is abrogated by elongation of mouse MHC class I. While investigating the possible mechanism(s) underlying this effect, we were unable to rule out the possibility that elongation was affecting binding of CD8 to MHC class I. A key difficulty was that the murine T cell systems we used were entirely dependent on coreceptor binding (data not shown). We therefore extended our analysis to human T cell antigen recognition of HLA-A2 restricted antigens, because of the availability of HLA-A2-restricted T cells, which are less dependent on coreceptor engagement (30).

Normal length (A2SCT) and elongated (A2SCT-CD4) single chain trimer versions of HLA-A2 were expressed incorporating the peptide SLYNTVATL (SLY) from the human immunodeficiency virus, type 1 Gag p17 protein (Fig. 2*A*). We also expressed soluble versions of both proteins (sA2SCT and sA2SCT-CD4) for binding and functional studies. TAP-deficient CHO cells expressing A2SCT stimulated IFNγ production by the G10 T cell clone (24), confirming that this SLY/HLA-A2 SCT is recognized by cognate T cells (Fig. 2*B*). In contrast, cells expressing the elongated form of the SCT failed to stimulate IFNγ production (Fig. 2*B*). Analogous results were obtained using a T cell clone (SLY10) selected for its ability to recognize SLY/HLA-A2 independently of CD8 binding (26) and APC-expressing versions of A2SCT and A2SCT-CD4 that are unable to bind CD8 because of the introduction of mutations D227K and T228A in the CD8-binding site (Fig. 2*A*) (31). The elongated form of A2SCT(*dCD8) induced much less MIP1b production by SLY10 cells than the normal length A2SCT(*dCD8) (Fig. 2*C*), strongly indicating that the effects of pMHC elongation were unrelated to CD8 binding.

To investigate directly possible effects of pMHC elongation on coreceptor and TCR binding, we used surface plasmon resonance to measure the affinity of both CD8αα and G10 TCR binding to soluble A2SCT. Soluble CD8αα bound with comparable affinity to both A2SCT and A2SCT-CD4 (Fig. 2*D*), with a slightly higher affinity than the range reported previously for CD8αα binding to human MHC class I (32). Taken together with the data in Fig. 2*C*, these results show that elongation of pMHC class I abrogates antigen recognition by human T cells independently of any effect on CD8 binding. As expected, soluble G10 TCR binding to A2SCT and A2SCT-CD4 was comparable (Fig. 2*E*). There was no detectable binding of G10 TCR to a control pMHC complex; HLA-A2 assembled with the NY-ESO epitope (data not shown).

Effect of HLA-A2 Elongation on CD3 Clustering, Zap70 Recruitment and CD45 Segregation—To explore the mechanism by which HLA-A2 elongation affected T cell antigen recognition, we next investigated the effect of elongation of A2SCT on CD3 clustering, Zap70 recruitment, and CD45 segregation. To improve imaging resolution G10 T cells were incubated with surface-immobilized A2SCT before fixing and staining (Fig. 3 and supplemental Fig. S3). Incubation with A2SCT led to substantially greater recruitment of Zap70 to the contact interface than seen with elongated A2SCT (Fig. 3, *A* and *C*). There was also increased accumulation of total CD3 at the interface (Fig. 3, *A* and *B*), but this was mainly the result of an increase in the contact area (Fig. 3*A*). To control for this we measured the proportion of interface CD3 that was clustered (supplemental Fig. S4). Interestingly, A2SCT and elongated A2SCT stimulated the same degree of CD3 clustering (Fig. 3, *A* and *D*) consistent with similar degrees of TCR engagement. In support of this the tyrosine kinase inhibitor PP2 inhibited Zap70 recruitment but not CD3 clustering (Fig. 3*E*).

We next examined whether elongation of A2SCT affected segregation of TCR·CD3 from CD45. Whereas both A2SCT and elongated A2SCT decreased the degree of CD3 colocalization with CD45 compared with control ligand, CD3/CD45 colocalization was less with normal A2SCT compared with elongated A2SCT (Fig. 4), indicating that elongation of A2SCT reduced segregation (or enhanced colocalization) of TCR·CD3 and CD45.

DISCUSSION

The key finding reported here is that elongation of pMHC I abrogates T cell antigen recognition in several mouse and human TCR·pMHC systems, indicating that it is a general phenomenon. This is seen using several different early (tyrosine phosphorylation and Zap70 recruitment) and late (cytokine/chemokine production and cytotoxic killing) readouts of antigen recognition. Interestingly, elongation did not appear to abrogate cytotoxic killing of target cells when SCT were expressed at higher levels (Fig. 1*E*), at which effects were seen in other functional assays. However, elongation did inhibit killing when SCTs were expressed at much lower levels on target cells (Fig. 1*F*). One possible explanation for this suggested by previous studies (26–29) is that the threshold for stimulating killing by the highly differentiated, repeatedly stimulated CD8 T cells is so low that even reduced TCR signals induced by elongated SCT are sufficient for full killing. In support of such a threshold difference, we found that inhibition of killing required ~10-fold higher concentration of the tyrosine kinase inhibitor PP2 (Fig.

FIGURE 3. **TCR·CD3 triggering but not clustering is diminished by pMHC elongation.** *A*, clean poly-L-lysine coated coverslips were incubated at 37 °C for 2 h with 50 μg/ml streptavidin/PBS. Biotinylated SCTs were immobilized on coverslips at comparable densities (Fig. S3). G10 cells were placed on SCT-coated coverslips and incubated for 1 min at 37 °C. The cells were fixed and permeabilized before serial staining CD3, Zap70, and CD45. The images were acquired using uniform settings between experiments. The cells adhered poorly on uncoated coverslips; therefore coverslips coated with biotinylated anti-HLA antibody was used as a control surface (without cognate TCR ligands). The *scale bar* represents 4 μm. *B–D*, the mean intensities for CD3, Zap70, and CD45 accumulation at the T cell interface was quantified. For a better appreciation of regions of TCR clustering pseudocolor scaled images of the CD3 distribution are shown (CD3 Scale) in *A* and *E*. The regions of CD3 clustering were arbitrarily defined by thresholding at two times the mean CD3 fluorescence intensity at the T cell interface (corresponding to the *yellow regions* in the pseudocolored scale images) and expressed as percentages of total CD3 interface fluorescence (Fig. S4). *E*, G10 cells were incubated with 10 μM PP2 for 30 min prior to placing on to SCT-coated coverslips. Preparation and labeling were performed as described above. The *scale bar* represents 4 μm. The *horizontal black bars* represent the means. Statistical significance was determined by analysis of variance with correction for multiple comparisons. *ns*, $p > 0.05$; **, $p < 0.01$; ***, $p < 0.001$.

A

	CD3	CD45	Overlay
A2SCT			
A2SCT-CD4			
anti-HLA			

B
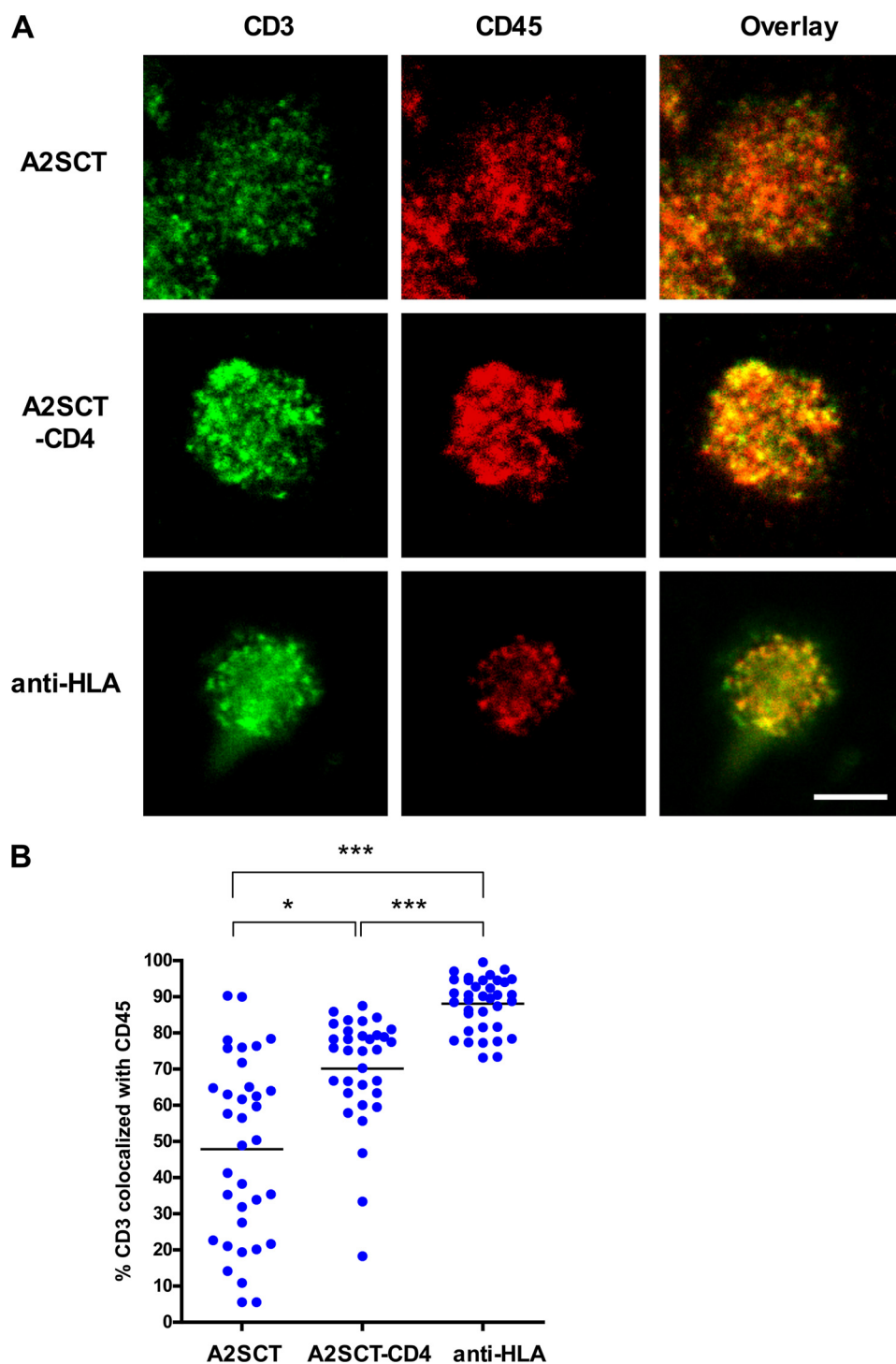
FIGURE 4. Small pMHC dimensions allow efficient segregation from CD45 following TCR engagement. *A*, experiments were performed as in Fig. 3. The data were acquired as 8-bit 1024 × 1024 pixel images. *B*, background subtracted images acquired in the CD3 and CD45 channels were analyzed for colocalization by determining Manders colocalization coefficients using ImageJ. The mean proportion of CD3 colocalized with CD45 expressed as a percentage (Manders M1 coefficient) was calculated from 20 interfaces chosen at random for each coated surface. Manders M2 coefficient (proportion of CD45 colocalized with CD3) is 100% for all. The *horizontal black bars* represent the means. Statistical significance was determined by analysis of variance with correction for multiple comparisons. *, $p < 0.05$; ***, $p < 0.001$. The *scale bar* represents 4 μm.

Elongation Does Not Affect TCR or Coreceptor Engagement—One trivial explanation for the inhibition of antigen recognition by elongation is that elongation of pMHC disrupts TCR and/or coreceptor binding. Several lines of evidence presented here indicate that this is not the case. First, enrichment of SCT at the T cell/APC contact interface and clustering of CD3 upon binding SCT was comparable with both normal and elongated SCT (Figs. 1*D* and 3*D*), indicating that TCR engagement was unaffected. Second, elongated and normal length forms of soluble SCT bound both soluble G10 TCR and CD8 with the same affinities (Figs. 2, *D* and *E*). Finally, antigen recognition of an SCT mutant unable to bind to CD8 was also greatly inhibited by elongation (Fig. 2*C*).

Segregation of CD45 from CD3 within the Contact Area—One possible mechanism by which elongation of pMHC might abrogate TCR triggering is by allowing greater access of engaged TCR to CD45. We previously examined this possibility by looking at the surface density of T cell CD45 at the contact interface (21). Our analysis was compromised by the low resolution of the imaging and the fact that TCR triggering can lead to an increase in total CD45 at the contact interface, probably as a result of increase membrane ruffling or active transport of CD45. Only when TCR triggering was inhibited was it possible to demonstrate CD45 depletion from the contact interface, and that elongation abrogated this exclusion (21). In this study we examined the relative distribution of CD45 and CD3 at higher resolution using surface immobilized SCT. Under these conditions elongation of SCT increased CD45 colocalization with CD3, indicating that segregation was less efficient (Fig. 4).

Effect of Elongation on Intermembrane Distance—Previously we have shown that elongation of H-2K[b] SCT by insertion of the four Ig domains from CD4 ($\sim$12 nm) resulted in an increase in the intermembrane distance between the T cell and APC. An interesting finding, however, was that the average intermembrane distance was increased by

1*G*). An alternative explanation for the observation that killing was not as susceptible to elongation as other assays is that different TCR triggering mechanism(s) may be involved in evoking different functional responses.

only ~5 nm, and there was a wider variation in the intermembrane distance. In the present study we extended this analysis to the H-2D^b SCT and compared the effect of inserting two or four Ig domains on intermembrane distance (supplemental Fig. S2). As before, the increase in intermembrane distance was smaller than expected, and there was more variation with longer SCTs. These results support the notion that the elongated SCTs are not fully extended and are flexible. The fact that insertion of CD2 leads to a fairly small increase in intermembrane distance as measured by EM, despite having a large effect on antigen recognition, raises the possibility that elongation may be inhibiting TCR triggering by a mechanism that does not require an increase in intermembrane distance.

It has recently been pointed out that the TCR·pMHC interaction will be subjected to mechanical force (13) and that the pulling force imposed by pMHC binding to TCR could lead to a conformational change in the TCR·CD3 complex that could contribute to TCR triggering (14, 16, 17). Were such a mechanism to operate, then elongation of pMHC without an equivalent increase in intermembrane distance would decrease the pulling force applied to the TCR and thereby abrogate triggering.

In conclusion, the TCR·pMHC complex is relatively small compared with other abundant cell surface molecules. Our findings reported here confirm that TCR triggering in CD8 cells is critically dependent on the small size of its pMHC I ligand. One potential reason for this is that this small size allows engagement to occur in areas of very close cell-cell contact from which CD45 is excluded, as proposed in the kinetic segregation model. This explanation is supported by our observation that elongating pMHC increases the intermembrane distance and CD45/CD3 colocalization at the contact interface. A second potential explanation for the inhibitory effect of elongation is that it reduces the pulling force that the TCR is subjected to upon binding to pMHC. Further experiments are required to fully elucidate the precise mechanism(s).

REFERENCES

1. Davis, M. M., and Chien, Y. H. (2003) in *Fundamental Immunology* (Paul, W. E., ed) pp. 227–258, Lippincott Williams & Wilkins, Philadelphia, PA
2. Weiss, A., and Samelson, L. E. (2003) in *Fundamental Immunology* (Paul, W. E., ed) pp. 321–364, Lippincott Williams & Wilkins, Philadelphia, PA
3. Springer, T. A. (1990) *Nature* **346,** 425–434
4. van der Merwe, P. A., McNamee, P. N., Davies, E. A., Barclay, A. N., and Davis, S. J. (1995) *Curr. Biol.* **5,** 74–84
5. Barclay, A. N., Brown, M. H., Law, S. K., McKnight, A. J., Tomlinson, M. G., and van der Merwe, P. A. (1997) *The Leucocyte Antigen Facts Book*, 2nd Ed., Academic Press, London
6. Davis, S. J., and van der Merwe, P. A. (1996) *Immunol. Today* **17,** 177–187
7. Weiss, A., and Littman, D. R. (1994) *Cell* **76,** 263–274
8. Davis, M. M., Krogsgaard, M., Huse, M., Huppa, J., Lillemeier, B. F., and Li, Q. J. (2007) *Annu. Rev. Immunol.* **25,** 681–695
9. Davis, S. J., and van der Merwe, P. A. (2006) *Nat. Immunol.* **7,** 803–809
10. Kuhns, M. S., Davis, M. M., and Garcia, K. C. (2006) *Immunity* **24,** 133–139
11. Schamel, W. W., Risueño, R. M., Minguet, S., Ortíz, A. R., and Alarcón, B. (2006) *Trends Immunol.* **27,** 176–182
12. Trautmann, A., and Randriamampita, C. (2003) *Trends Immunol.* **24,** 425–428
13. van der Merwe, P. A. (2001) *Immunity* **14,** 665–668
14. Choudhuri, K., and van der Merwe, P. A. (2007) *Semin. Immunol.* **19,** 255–261
15. Rudolph, M. G., Stanfield, R. L., and Wilson, I. A. (2006) *Annu. Rev. Immunol.* **24,** 419–466
16. Choudhuri, K., Kearney, A., Bakker, T. R., and van der Merwe, P. A. (2005) *Curr. Biol.* **15,** R382–385
17. Ma, Z., Janmey, P. A., and Finkel, T. H. (2008) *FASEB J.* **22,** 1002–1008
18. Beddoe, T., Chen, Z., Clements, C. S., Ely, L. K., Bushell, S. R., Vivian, J. P., Kjer-Nielsen, L., Pang, S. S., Dunstone, M. A., Liu, Y. C., Macdonald, W. A., Perugini, M. A., Wilce, M. C., Burrows, S. R., Purcell, A. W., Tiganis, T., Bottomley, S. P., McCluskey, J., and Rossjohn, J. (2009) *Immunity* **30,** 777–788
19. Xu, C., Gagnon, E., Call, M. E., Schnell, J. R., Schwieters, C. D., Carman, C. V., Chou, J. J., and Wucherpfennig, K. W. (2008) *Cell* **135,** 702–713
20. van der Merwe, P. A., Davis, S. J., Shaw, A. S., and Dustin, M. L. (2000) *Semin. Immunol.* **12,** 5–21
21. Choudhuri, K., Wiseman, D., Brown, M. H., Gould, K., and van der Merwe, P. A. (2005) *Nature* **436,** 578–582
22. Palmowski, M. J., Parker, M., Choudhuri, K., Chiu, C., Callan, M. F., van der Merwe, P. A., Cerundolo, V., and Gould, K. G. (2009) *J. Immunol.* **182,** 4565–4571
23. Wyer, J. R., Willcox, B. E., Gao, G. F., Gerth, U. C., Davis, S. J., Bell, J. I., van der Merwe, P. A., and Jakobsen, B. K. (1999) *Immunity* **10,** 219–225
24. Lee, J. K., Stewart-Jones, G., Dong, T., Harlos, K., Di Gleria, K., Dorrell, L., Douek, D. C., van der Merwe, P. A., Jones, E. Y., and McMichael, A. J. (2004) *J. Exp. Med.* **200,** 1455–1466
25. Mamalaki, C., Norton, T., Tanaka, Y., Townsend, A. R., Chandler, P., Simpson, E., and Kioussis, D. (1992) *Proc. Natl. Acad. Sci. U.S.A.* **89,** 11342–11346
26. Laugel, B., Price, D. A., Milicic, A., and Sewell, A. K. (2007) *Eur. J. Immunol.* **37,** 905–913
27. Price, D. A., Sewell, A. K., Dong, T., Tan, R., Goulder, P. J., Rowland-Jones, S. L., and Phillips, R. E. (1998) *Curr. Biol.* **8,** 355–358
28. Valitutti, S., Müller, S., Dessing, M., and Lanzavecchia, A. (1996) *J. Exp. Med.* **183,** 1917–1921
29. Sykulev, Y., Joo, M., Vturina, I., Tsomides, T. J., and Eisen, H. N. (1996) *Immunity* **4,** 565–571
30. Hutchinson, S. L., Wooldridge, L., Tafuro, S., Laugel, B., Glick, M., Boulter, J. M., Jakobsen, B. K., Price, D. A., and Sewell, A. K. (2003) *J. Biol. Chem.* **278,** 24285–24293
31. Purbhoo, M. A., Boulter, J. M., Price, D. A., Vuidepot, A. L., Hourigan, C. S., Dunbar, P. R., Olson, K., Dawson, S. J., Phillips, R. E., Jakobsen, B. K., Bell, J. I., and Sewell, A. K. (2001) *J. Biol. Chem.* **276,** 32786–32792
32. van der Merwe, P. A., and Davis, S. J. (2003) *Annu. Rev. Immunol.* **21,** 659–684